Crystallography, spectroscopic analysis, and lasing properties of $Nd^{3+}:Y_3Sc_2Al_3O_{12}$

Toomas H. Allik
Science Applications International Corporation, 1710 Goodridge Drive, McLean, Virginia 22102

Clyde A. Morrison
U.S. Army Electronics Research and Development Command, Harry Diamond Laboratories, Adelphi, Maryland 20783-1197

John B. Gruber
Department of Physics, San Jose State University, San Jose, California 95192-0106

Milan R. Kokta
Union Carbide Corporation, 750 South 32nd Street, Washougal, Washington 98671
(Received 21 June 1989)

The crystallographic, optical, and spectroscopic properties of $Nd^{3+}:Y_3Sc_2Al_3O_{12}$ are reported from which an assessment can be made regarding the material's potential as a laser. Individual Stark levels for many of the $^{2S+1}L_J$ manifolds of $Nd^{3+}(4f^3)$ in the crystal have been identified from emission and absorption data up to 17 600 cm^{-1} at 14 K. The observed crystal-field splitting and the measured cross sections (intensities) associated with manifold-to-manifold transitions are compared with calculated splittings and calculated intensities. The crystal-field and Judd-Ofelt intensity parameters were calculated for Nd and all other rare-earth ions. Branching ratios and diode-array-pumped laser slope efficiencies are also reported. We conclude that $Nd^{3+}:Y_3Sc_2Al_3O_{12}$ has potential as a diode-pumped one-micrometer laser material.

I. INTRODUCTION

Increasing demands placed on solid-state lasers in applications ranging from communications to medicine highlight the need to develop new materials that have better diode-pump-laser characteristics than the standard laser material Nd: yttrium aluminum garnet (YAG).[1-9] The challenge is made clear with the present availability of single-laser diodes with powers exceeding 1 W and two-dimensional arrays producing intensities of more than 4 kW/cm^2 at the required wavelength. Desirable properties of new diode-pumped Q-switched solid-state lasers include a longer fluorescent lifetime and a larger absorption coefficient than is possible with Nd:YAG. In addition, the optical, mechanical, and thermal crystal properties of the host must be competitive with Nd:YAG to permit high-repetition-rate applications.

There are several reasons for examining the laser properties of $Nd:Y_3Sc_2Al_3O_{12}$ (YSAG) in greater detail.[10-12] The distribution coefficient for Nd^{3+} in YSAG is roughly twice that for YAG,[13,14] making it possible to increase the Nd^{3+} concentration in YSAG over that in YAG. Replacing Al^{3+} ions with larger Sc^{3+} ions increases the distance between dodecahedral lattice sites (substitutional sites for Nd^{3+} ions in the garnet structure). Any increase in separation between neighboring Nd^{3+} ions, especially with increasing concentration, tends to reduce the relatively strong ion-ion interaction in YAG, which leads to concentration quenching of the Nd^{3+} fluorescence.[10,15,16] In addition, the aluminum-based systems, such as YAG, YSAG, or gadolinium scandium aluminum garnet (GSAG), are formed from more stable constituent oxides than gallium-containing materials, such as GGG. The tendency for color center formation in gallium-containing garnets is due to oxidation state variation or oxygen vacancies, and this problem is greatly reduced in aluminate systems.

Only some of the spectroscopic properties of Nd:YSAG have been reported in the open literature.[10,17] Kaminskii reports energy levels up to the $^4F_{3/2}$ manifold only.[10] Most of the literature concentrates on the empirical evaluation of Nd:YSAG and Cr^{3+} sensitized Nd:YSAG as a laser.[11,12,18,19] However, to fully assess the potential of this material, it is important to study the spectroscopic properties in greater detail. The individual experimental Stark levels and the measured cross sections and lifetimes of transitions between these levels should be compared with theoretical predictions based on lattice-sum calculations, crystal-field splitting, and the predicted cross sections and lifetimes based on the Judd-Ofelt model for rare-earth ions in solids.[16,20-22]

We report here the results of crystal growth and x-ray diffraction studies, along with measurements on the index of refraction of Nd:YSAG. The experimental Stark levels for many of the $^{2S+1}L_J$ manifolds of $Nd^{3+}(4f^3)$ deduced from both absorption and emission data are tabulated up to 17 600 cm^{-1} and compared with a theoretical crystal-field splitting calculation. A survey spectrum of Nd:YSAG between 300 and 1000 nm and the fluorescence from $^4F_{3/2}$ to $^4I_{11/2}$, both obtained at room temperature, provide a general overview of observed optical properties of Nd^{3+}. Absorption intensities from the ground-state manifold of Nd^{3+} ($^4I_{9/2}$) to excited manifolds observed in the survey spectrum are compared with

calculated intensities based on the Judd-Ofelt theory.[20–22] Branching ratios and slope efficiencies are also reported from which an assessment can be made regarding Nd:YSAG as a laser material.

II. EXPERIMENTAL RESULTS AND DISCUSSION

A. Crystal growth and structure

Yttrium scandium aluminum garnet belongs to the group of oxide compounds crystallizing in garnet structure. The first garnet containing scandium was synthesized by Moronova and Feofilov,[23] and a systematic study of Sc incorporation into aluminum garnets was made by Kokta[13] in 1973. Subsequently, a scandium-substituted rare-earth aluminum garnet (GSAG) was grown by Brandle and Venderleeden.[24] An interest in scandium-substituted garnets was revived a decade later when their usefulness as tunable solid-state laser hosts was demonstrated with Cr^{3+}-doped in GSGG.[25]

The first crystals of yttrium scandium aluminum garnets doped either with neodymium and/or chromium were grown in a 2×2 in.^{2} crucible. They were approximately 0.9 in. in diameter and 2 in. long. These crystals were used to fabricate spectroscopic samples as well as seeds for further crystal growth.

For laser application, a 5-in. long Nd-doped crystal of 1.5 in. diameter was grown. The furnace used to grow this material was built from a silica sleeve inserted in an rf coil. A 3×3in.^{2} iridium crucible was used which was surrounded by a 3.5 in. I.D. zirconium oxide liner. The space between the ZrO_2 liner and the SiO_2 sleeve was filled with insulation consisting of zirconium oxide bubbles (grog). The induction coil, which was made from $\frac{3}{8}$ in. diameter copper tubing, was wound into 12 turns around the growth furnace, and powered by a 50-kW motor generator operating at a 10-kHz frequency. The crucible was filled in the 3:2:3 molar ratio for Y_2O_3, Sc_2O_3, and Al_2O_3. The amount of Nd_2O_3 was calculated for substitution of 1.5 at. % Nd into eightfold-coordination sites, under the assumption that the Nd distribution coefficient, k_{Nd}, approached 0.4 in this system. However, the Nd concentration of a spectroscopic sample from the boule was determined by x-ray fluorescence to be 1.76 ± 0.10 wt. %, which corresponds to a Nd density of $(3.33\pm0.07)\times10^{19}$ cm^{-3}.[26] The deviation between the measured and calculated Nd concentration is not surprising, since the exact value of k_{Nd} is a growth dependent parameter (rotation rate, pull rate). More growth runs would be required to determine k_{Nd} precisely for given growth conditions.

The crystals were grown along the ⟨111⟩ orientation, at a rate of 0.015 in./hr, and were rotated at 15 RPM. They were grown under an ambient atmosphere of nitrogen containing 800 ppm by volume of O_2. The melting point was determined with an optical pyrometer to be 1900 ± 25 °C, uncorrected for emissivity. YSAG showed typical garnet faceting as observed in YAG crystals. The interface shape was convex, and strain was observed in the "core" area. No attempts were made to change the interface shape. The strain pattern is significantly more pronounced in YSAG than is the strain in YAG. YSAG crystals have a much higher tendency to crack, and therefore extreme caution must be exercised during their fabrication. Contrary to the findings of Brandle,[24] a slower pull rate seems to ease this problem, and rates even lower than 0.015 in./h may be well justified, especially for crystals doped with Nd.

The crystal structure analysis was performed on an automated Nicolet $R3m/\mu$ diffractometer equipped with an incident-beam graphite monochromator and Mo K_α radiation ($\lambda=0.7107$ Å). Single-crystal diffraction patterns of the crystal showed that the crystals were cubic, belonging to the space group $Ia\bar{3}d$ (No. 230), with a unit-cell axis length of $a=12.271$ Å ($V=1847.6$ Å^3). The lattice parameter differs from that of Kokta[13] ($a=12.324$ Å) and Bogomolova[27] ($a=12.251$ Å); this difference is attributed to the distribution coefficient for Sc being less than unity, which allows for mixed occupancy between Sc and Al in the octahedral site. This should allow ranges in lattice parameters from stoichiometric YSAG ($a=12.32$ Å) to YAG ($a=12.00$ Å). Elemental analysis performed on the sample by x-ray fluorescence did indeed show lower Sc than expected in the crystal.[26] The 191 independent single-crystal reflections recorded were used to refine the structure by least squares to residuals of $R=0.0342$ and $wR=0.0502$. Positional and thermal parameters are tabulated in Table I. Further details on the data collection and on the crystal structure are given by Campana.[28]

B. Index of refraction

The refractive indices of Nd:YSAG were measured using the method of minimum deviation.[29] A polished prism of Nd:YSAG was fabricated to a height of 5 mm and had faces of 12 and 17 mm. The prism angle was 44° 55′. A Spencer 2754 Spectrometer (American Optical Company) was used to make all angular measurements, and multiline argon ion and helium neon lasers were used as light sources between 457.9 and 632.8 nm. The measured refractive indices are given in Table II. The accuracy of these measurements was ±0.002 because of the poor optical quality of the sample.

These experimental data were least-squares fit to Sellmeier's dispersion equation

$$n(\lambda)^2=1+A\lambda^2/(\lambda^2-B)\,, \tag{1}$$

where $A=2.420\pm0.008$ and $B=0.015\,20\pm0.000\,64\ \mu m^2$.

TABLE I. Atom coordinates ($\times10^4$) and thermal coefficients (Å$^2\times10^3$) of $Y_3Sc_2Al_3O_{12}$.

Atom	x	y	z	U^a_{eq}
Y	0	0	0	74(4)
Sc	0	2500	1250	51(3)
Al	0	2500	3750	41(7)
O	309(3)	562(3)	6562(3)	67(9)

[a]Equivalent isotropic U defined as one third of the trace of the orthogonalized U_{ij} tensor. Parenthetical values are estimated standard deviations.

TABLE II. Measured and calculated indices of refraction of Nd^{3+}:$Y_3Sc_2Al_3O_{12}$ at 298 K.

Wavelength	n_{meas}	n_{calc}
457.9	1.900	1.900
476.5	1.895	1.896
488.0	1.893	1.893
496.5	1.891	1.892
514.5	1.889	1.889
594.5	1.880	1.878
611.9	1.878	1.877
632.8	1.873	1.875

Crystal	Sellmeier coefficients	
	A	B
Nd:YSAG	2.420	0.01520
YSAG (Ref. 30)	2.4118	0.01477

These results agree well with the results of Wemple and Tabor for undoped YSAG.[30] The refractive indices for the doped sample are higher than the ones for the undoped.

C. Nd^{3+} absorption

The absorption spectrum of neodymium-doped YSAG was investigated in the range from 1500 to 40 000 cm^{-1}. These data were recorded in the ultraviolet, visible, and infrared on Perkin-Elmer Lambda 9 and 983 G spectrometers interfaced to the Perkin-Elmer 7500 computer. Figure 1 shows the room-temperature absorption spectrum between 300 and 1000 nm of a 2.95 mm long, Nd^{3+}:YSAG sample with the Fresnel reflection losses removed. Well-resolved Stark levels exhibited Gaussian line shapes indicative of inhomogeneous broadening. The FWHM of these transitions were 30–40 cm^{-1}.

Determination of the individual Stark levels of the Nd^{3+} ions in the dodecahedral sites (D_2 symmetry) was accomplished by cooling the sample to cryogenic temperatures. A closed-cycle refrigerator, CTI-Cryogenics Model 21, was used to obtain spectra at 14 K. Table III lists the 60 lowest experimentally determined energy levels (up to 17 600 cm^{-1}). Energy levels up to 40 000 cm^{-1} have been determined and are currently being fit to a theoretical crystal-field calculation, which includes spin-correlation effects; this calculation will be reported at a later date.[31] The low-lying energy levels, up to $^4F_{3/2}$, agree very well with those of Kaminskii.[10] The overall accuracy of the measurements is ≤ 5 cm^{-1}.

D. Nd^{3+} fluorescence

The fluorescence spectrum of Nd^{3+}:YSAG was recorded with a Spex F222 spectrometer equipped with a North Coast model EO-817L Ge detector. Figure 2 shows the fluorescence of Nd^{3+}:YSAG and, for comparison, Nd^{3+}:YAG in the region of the $^4F_{3/2} \rightarrow {}^4I_{11/2}$ ($R_{1,2} \rightarrow Y_{1-6}$) transitions. In general, the fluorescence lines of Nd:YSAG show a broadening versus YAG. At room temperature, the two most intense lines for Nd:YSAG appear at 1.0622 and 1.0595 μm. These wavelengths correspond to the $R_2 \rightarrow Y_3$ and $R_1 \rightarrow Y_1$ transitions, respectively. In addition to these two prominent lines, the $R_1 \rightarrow Y_2$ and $R_2 \rightarrow Y_4$ transitions appear as shoulders on the long-wavelength side of the band. The individual Stark-level branching ratios were estimated from the peak heights to be 15% for $R_2 \rightarrow Y_3$ and 13% for $R_1 \rightarrow Y_1$. Accurate determinations of the distributions were not possible because of the limited resolution of the monochromator. An estimate of the $R_2 \rightarrow Y_3$ transition bandwidth is 35 ± 10 cm^{-1} FWHM. This value is considerably larger than Kaminski's value[10] of 8 cm^{-1} and is indicative of considerable strain in our crystal.

The fluorescence lifetime of the $^4F_{3/2}$ state was measured using a $Ga_xAl_{1-x}As$ laser diode as the excitation source. The diode emits radiation at 805 nm at room temperature, and the pulse duration was 2 μs. Fluorescence detection was viewed through an 850-*nm* long-pass filter into an Si detector. Signals were processed by a Stanford Research Systems boxcar integrator and stored in a computer. The fluorescence lifetime at room temperature was 208 ± 5 μs at an Nd concentration of 1.76

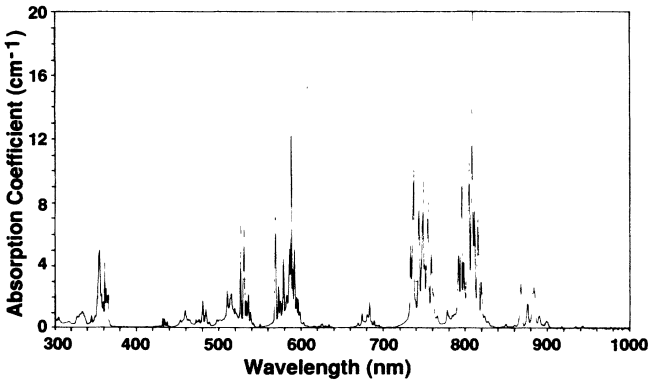

FIG. 1. Room-temperature absorption spectrum of Nd^{3+}:YSAG. The Nd concentration is 3.3×10^{19} cm^{-3}.

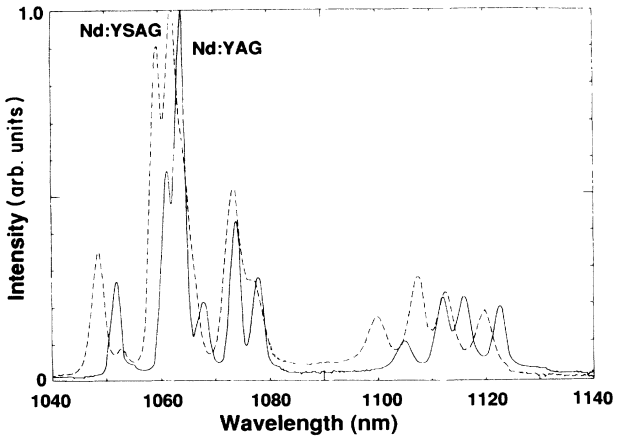

FIG. 2. $^4F_{3/2} \rightarrow {}^4I_{11/2}$ fluorescence spectra of Nd^{3+} doped in YSAG and YAG at room temperature.

TABLE III. Experimental and theoretical crystal-field splittings of Nd^{3+} ion manifolds in YSAG.

	Energy (Expt. cm^{-1})	Energy (Theor. cm^{-1})	$^{2S+1}L_J$ (Centroid cm^{-1})	Free-ion mixture (%)
1	0	−11	$^4I_{9/2}$	98.18 $^4I_{9/2}$ + 1.40 $^4I_{11/2}$ + 0.27 $^4I_{13/2}$
2	114	120	(362)	98.08 $^4I_{9/2}$ + 1.38 $^4I_{11/2}$ + 0.39 $^4I_{13/2}$
3	183	188		96.68 $^4I_{9/2}$ + 3.06 $^4I_{11/2}$ + 0.09 $^4I_{13/2}$
4	301	300		95.70 $^4I_{9/2}$ + 4.06 $^4I_{11/2}$ + 0.07 $^4F_{3/2}$
5	823	824		97.68 $^4I_{9/2}$ + 2.04 $^4I_{11/2}$ + 0.20 $^4I_{13/2}$
6	1979	1982	$^4I_{11/2}$	96.98 $^4I_{11/2}$ + 2.31 $^4I_{13/2}$ + 0.30 $^4I_{15/2}$
7	2022	2016	(2222)	95.12 $^4I_{11/2}$ + 2.77 $^4I_{13/2}$ + 1.81 $^4I_{9/2}$
8	2101	2104		96.78 $^4I_{11/2}$ + 2.07 $^4I_{13/2}$ + 0.77 $^4I_{9/2}$
9	2136	2131		96.82 $^4I_{11/2}$ + 2.47 $^4I_{13/2}$ + 0.42 $^4I_{9/2}$
10	2437	2442		93.83 $^4I_{11/2}$ + 4.38 $^4I_{9/2}$ + 1.58 $^4I_{13/2}$
11	2495	2495		95.11 $^4I_{11/2}$ + 4.10 $^4I_{9/2}$ + 0.61 $^4I_{13/2}$
12	3905	3906	$^4I_{13/2}$	97.08 $^4I_{13/2}$ + 2.48 $^4I_{15/2}$ + 0.14 $^4I_{11/2}$
13	3929	3923	(4188)	95.92 $^4I_{13/2}$ + 2.34 $^4I_{15/2}$ + 1.42 $^4I_{11/2}$
14	4029	4036		97.90 $^4I_{13/2}$ + 1.33 $^4I_{15/2}$ + 0.35 $^4I_{11/2}$
15	4044	4042		96.58 $^4I_{13/2}$ + 2.36 $^4I_{15/2}$ + 0.67 $^4I_{11/2}$
16	4057[a]	4411		96.20 $^4I_{13/2}$ + 2.88 $^4I_{11/2}$ + 0.53 $^4I_{15/2}$
17	4419	4420		94.25 $^4I_{13/2}$ + 3.25 $^4I_{11/2}$ + 2.16 $^4I_{15/2}$
18	4478	4478		95.96 $^4I_{13/2}$ + 2.76 $^4I_{11/2}$ + 0.91 $^4I_{15/2}$
19	5766	5772	$^4I_{15/2}$	97.68 $^4I_{15/2}$ + 1.95 $^4I_{15/2}$ + 0.10 $^4F_{9/2}$
20	5797	5794	(6221)	99.08 $^4I_{15/2}$ + 0.51 $^4I_{13/2}$ + 0.13 $^4F_{9/2}$
21	5927	5924		98.75 $^4I_{15/2}$ + 0.77 $^4I_{13/2}$ + 0.14 $^4F_{9/2}$
22	5981	5988		98.57 $^4I_{15/2}$ + 0.85 $^4I_{13/2}$ + 0.21 $^4F_{9/2}$
23	6544	6539		97.20 $^4I_{15/2}$ + 2.48 $^4I_{13/2}$ + 0.08 $^4I_{11/2}$
24	6560	6563		98.48 $^4I_{15/2}$ + 1.03 $^4I_{13/2}$ + 0.43 $^4I_{11/2}$
25	6622	6625		97.56 $^4I_{15/2}$ + 2.12 $^4I_{13/2}$ + 0.13 $^4I_{11/2}$
26	6711	6704		97.42 $^4I_{15/2}$ + 2.24 $^4I_{13/2}$ + 0.25 $^4F_{7/2}$
27	11 423	11 431	$^4F_{3/2}$	93.77 $^4F_{3/2}$ + 2.80 $^4F_{5/2}$ + 1.35 $^2H_{9/2}$
28	11 523	11 515	(11 523)	93.44 $^4F_{3/2}$ + 3.54 $^4F_{5/2}$ + 1.45 $^4F_{7/2}$
29	12 382	12 367	$^4F_{5/2}$	77.45 $^4F_{5/2}$ + 13.84 $^2H_{9/2}$ + 3.96 $^4F_{7/2}$
30	12 441	12 435	(12524)	61.74 $^2H_{9/2}$ + 32.80 $^4F_{5/2}$ + 3.17 $^4F_{3/2}$
31	12 538[a]	12 456		65.56 $^2H_{9/2}$ + 29.23 $^4F_{5/2}$ + 2.90 $^4F_{3/2}$
32	12 583	12 590		75.52 $^2H_{9/2}$ + 23.52 $^4F_{5/2}$ + 0.20 $^4F_{3/2}$
33	12 621	12 633		95.97 $^4F_{5/2}$ + 2.41 $^2H_{9/2}$ + 0.62 $^4F_{7/2}$
34	12 637[a]	12 690	$^2H_{9/2}$	88.30 $^2H_{9/2}$ + 10.59 $^4F_{5/2}$ + 0.29 $^2H_{11/2}$
35	12 825	12 817	(12 664)	92.38 $^2H_{9/2}$ + 6.91 $^4F_{5/2}$ + 0.17 $^4F_{3/2}$
36	12 860	12 869		93.27 $^2H_{9/2}$ + 5.82 $^4F_{5/2}$ + 0.18 $^2H_{11/2}$
37	13 367	13 361	$^4F_{7/2}$	88.58 $^4F_{7/2}$ + 4.65 $^4F_{5/2}$ + 2.21 $^4S_{3/2}$
38	13 441	13 451	(13 490)	87.90 $^4F_{7/2}$ + 4.68 $^4S_{3/2}$ + 3.09 $^4F_{5/2}$
39	13 570	13 562		58.76 $^4S_{3/2}$ + 39.38 $^4F_{7/2}$ + 0.58 $^4G_{5/2}$
40	13 580	13 588		95.55 $^4S_{3/2}$ + 2.90 $^4F_{7/2}$ + 0.41 $^2H_{11/2}$
41	13 602	13 594	$^4S_{3/2}$	63.68 $^4F_{7/2}$ + 35.15 $^4S_{3/2}$ + 0.28 $^2H_{11/2}$
42	13 642	13 647	(13 588)	98.04 $^4F_{7/2}$ + 0.58 $^4S_{3/2}$ + 0.36 $^4I_{15/2}$
43	14 630	14 650	$^4F_{9/2}$	98.65 $^4F_{9/2}$ + 1.60 $^4F_{7/2}$ + 0.57 $^4F_{5/2}$
44	14 695	14 696	(14 756)	96.21 $^4F_{9/2}$ + 2.28 $^4F_{7/2}$ + 0.60 $^4F_{5/2}$
45	14 786	14 794		97.14 $^4F_{9/2}$ + 0.97 $^2H_{11/2}$ + 0.63 $^2G_{7/2}$
46	14 834	14 820		97.51 $^4F_{9/2}$ + 0.99 $^2H_{11/2}$ + 0.59 $^2G_{7/2}$
47	14 939	14 924		98.18 $^4F_{9/2}$ + 1.23 $^2G_{7/2}$ + 0.16 $^4F_{7/2}$
48	15 770[a]	15 892	$^2H_{11/2}$	97.34 $^2H_{11/2}$ + 2.11 $^2G_{7/2}$ + 0.27 $^4G_{5/2}$
49	15 860[a]	15 930	(15 971)	97.76 $^2H_{11/2}$ + 1.76 $^2G_{7/2}$ + 0.19 $^4F_{9/2}$
50	15 886[a]	15 959		98.95 $^2H_{11/2}$ + 0.39 $^2G_{7/2}$ + 0.21 $^2H_{9/2}$
51	15 964	15 964		98.68 $^2H_{11/2}$ + 0.53 $^2G_{7/2}$ + 0.32 $^4F_{9/2}$
52	16 093[a]	16 022		96.11 $^2H_{11/2}$ + 1.97 $^2G_{7/2}$ + 1.05 $^4F_{9/2}$
53	16 124[a]	16 067		96.69 $^2H_{11/2}$ + 1.30 $^4F_{9/2}$ + 1.15 $^2G_{7/2}$

TABLE III. (*Continued*).

	Energy (Expt. cm^{-1})	Energy (Theor. cm^{-1})	$^{2S+1}L_J$ (Centroid cm^{-1})	Free-ion mixture (%)
54	16 880	16 893	$^4G_{5/2}$	56.29 $^4G_{5/2}$ + 41.53 $^2G_{7/2}$ + 1.34 $^2H_{11/2}$
55	17 010	17 000	(17 090)	86.51 $^4G_{5/2}$ + 10.87 $^2G_{7/2}$ + 0.74 $^4S_{3/2}$
56	17 065	17 067	$^2G_{7/2}$	73.89 $^4G_{5/2}$ + 22.91 $^2G_{7/2}$ + 0.98 $^2H_{11/2}$
57	17 262	17 231	(17 192)	93.32 $^2G_{7/2}$ + 2.87 $^4G_{5/2}$ + 2.14 $^2H_{11/2}$
58	17 286	17 303		95.89 $^2G_{7/2}$ + 1.81 $^2H_{11/2}$ + 1.56 $^4G_{5/2}$
59	17 331	17 341		88.78 $^2G_{7/2}$ + 8.22 $^4G_{5/2}$ + 1.91 $^2H_{11/2}$
60	17 587[a]	17 664		65.32 $^4G_{5/2}$ + 34.12 $^2G_{7/2}$ + 0.16 $^2H_{11/2}$

[a]Experimental energy levels not used in the crystal-field calculations.

wt. %. A comparable Nd concentration in YAG would have a lifetime of 160 μs.[10]

E. Judd-Ofelt theory

Application of Judd-Ofelt (JO) theory[20,21] has become a valuable model in predicting rare-earth laser performance. The model was first successfully applied to individual Stark levels in the ethylsulfate system by Axe[32] (Eu^{3+}) and by Krupke and Gruber[33] (Tm^{3+}). Since then JO theory has been used by numerous laboratories to calculate the branching ratios, radiative lifetimes, and eventually stimulated emission cross sections of the $^4F_{3/2} \rightarrow {}^4I_J$ ($J=\frac{9}{2}$, $\frac{11}{2}$, $\frac{13}{2}$, and $\frac{15}{2}$) transitions. Detailed theoretical and experimental procedures are contained in works by Krupke,[34,35] Weber,[36] DeShazer,[37,38] and Kaminskii.[10,16] The JO model is based on the following relationship: the line strength, $S(J,J')$, for a transition between an initial J manifold $|4f^n[SL]J\rangle$ and final J' manifold $|4f^n[S'L']J'\rangle$ can be written in the form

$$S(J,J')=\sum_{t=2,4,6}\Omega_t|\langle 4f^n[SL]J\|U^{(t)}\|4f^n[S'L']J'\rangle|^2 , \tag{2}$$

where $|\langle\|U^{(t)}\|\rangle|^2$ are the squares of the transition-matrix elements for intermediate coupling from the ground state to the excited manifold, and Ω_t are the three phenomenological JO parameters. The numerical values of the transition-matrix elements for Nd^{3+} were taken from DeShazer.[37]

In practice, the integrated absorption coefficient, $\Gamma=\int\alpha(\lambda)d\lambda$, emanating from the ground state, $^4I_{9/2}$ manifold, was measured for 11 absorption bands using Fig. 1. The integrated absorption coefficient in turn is related to the line strength S by Eq. (3):

$$\Gamma=[8\pi^3N\bar{\lambda}e^2/3ch(2J+1)][(n^2+2)^2/9n]S(J,J') , \tag{3}$$

where N is the Nd^{3+} concentration, J is the total angular momentum quantum number of the initial level, $\bar{\lambda}$ is the mean wavelength, and n is the index of refraction. We assume in this calculation that all the Nd^{3+} goes in the dodecahedral site. The values for n were taken from Sellmeier's dispersion equation, Eq. (1). When the absorption band was a superposition of lines assigned to several intermultiplet transitions, the matrix element was taken to be the sum of the corresponding squared matrix elements. The JO parameters were obtained by minimizing the sum of the squared differences between S_{meas} and S_{calc}. Table IV shows Γ, n, S_{meas}, and S_{calc} for 11 absorption bands. The rms error of these calculations was 14%.

Once the JO parameters are known, S_{calc} was determined for transitions between $^4F_{3/2}$ and ^4I_J using the matrix elements emanating from the metastable $^4F_{3/2}$ state.[34] The total spontaneous emission probability $A(J,J')$ was calculated from:

$$A(J,J')=[64\pi^4e^2/3h(2J+1)\bar{\lambda}^3]\times[n(n^2+2)^2/9]S(J,J') , \tag{4}$$

and the intermanifold branching ratio $\beta(J,J')$ is given by

$$\beta(J,J')=A(J,J')/\sum_{J'}A(J,J') . \tag{5}$$

The JO parameters and the predicted branching ratios are given in Table V for Nd:YSAG. For comparison, the JO parameters and both the predicted and experimentally determined branching ratios[39] for Nd:YAG are given. It is interesting to note that the experimental JO parameters are virtually the same for both YSAG and YAG. These results in turn yield comparable radiative lifetimes of the $^4F_{3/2}$ upper laser levels and branching ratios to the ^4I_J states.

Finally, the stimulated-emission cross section σ_{21} for an inhomogeneously broadened linewidth (Gaussian lineshape) can be written as

$$\sigma_{21}=(A_{21}\lambda^2/4\pi n^2\Delta\nu)(\ln 2/\pi)^{1/2} . \tag{6}$$

The transition probability for the laser transition ($2\rightarrow1$) is given by the following expression:

$$A_{21}=[(1+\kappa)/\kappa](I_{21}/I_T)\tau_{rad}^{-1} , \tag{7}$$

where κ is the Boltzmann factor between the two levels of $^4F_{3/2}$, and I_{21}/I_T is the ratio of the photon rate for the laser transition to the photon rate of all transitions originating from either level of $^4F_{3/2}$. Using the experimentally determined values of $n=1.86$, $\lambda=1.0622\times10^{-4}$ cm, $\Delta\nu=35$ cm^{-1}, and $A_{21}=780$ s^{-1}, we determine the value

TABLE IV. Absorption intensities for Nd:YSAG at 298 K.

Excited state	Wavelength (nm)	n	Γ (nm/cm)	S_{meas}[a]	S_{calc}[a]
$^4F_{3/2}$	880	1.862	34.3	0.673	0.921
$^4F_{5/2},^2H_{9/2}$	805	1.865	159.2	3.408	3.177
$^4F_{7/2},^4S_{3/2}$	747	1.868	132.3	3.046	3.289
$^4F_{9/2}$	680	1.871	10.3	0.260	0.217
$^2H_{11/2}$	625	1.876	1.3	0.036	0.058
$^4G_{5/2},^2G_{7/2}$	583	1.880	75.8	2.213	2.242
$^4G_{7/2},^4G_{9/2},^2K_{13/2}$	520	1.888	50.9	1.655	1.253
$^2G_{9/2},^4G_{11/2},$ $^2K_{15/2},(^2D,^2P)_{3/2}$	470	1.897	17.4	0.621	0.310
$^2P_{1/2},^2D_{5/2}$	430	1.907	2.3	0.089	0.127
$^2P_{3/2}$	385	1.923	0.1	0.004	0.006
$^4D_{3/2},^4D_{1/2},^4D_{5/2},$ $^2I_{11/2}$	357	1.936	35.0	1.593	1.733

[a]In units of 10^{-20} cm^2, rms line strength (rms$-S$)$=1.705\times10^{-20}$ cm^2; rms deviation in line strength (rms$-\Delta S$)$=0.239\times10^{-20}$ cm^2; where (rms$-\Delta S$)$=[\sum(\Delta S^2)/$(No. of bands fitted$-$No. of parameters)$]^{1/2}$. $\sum$ = sum over all bands fitted.

of $\sigma(R_2\rightarrow Y_3)$ to be 9.1×10^{-20} cm^2. This value is considerably smaller than that for Nd:YAG (Ref. 35) (6.5×10^{-19} cm^2) and is attributable to both the inhomogeneity of the Nd^{3+} site due to the mixed occupancy between Sc and Al in the octahedral site and additional strain in our crystal.

F. Crystal-field calculations

The analysis of the experimental absorption data on Nd^{3+}:YSAG is the same as that of Nd^{3+}:LaLuGG given by Allik *et al.*[40] In these calculations, the experimentally determined Stark-level positions of Nd^{3+} given in Table III were used along with the free-ion Russell-Saunders $[SL]J$ states with the free-ion Hamiltonian containing the Coulomb, spin orbit, L^2, $G(G_2)$, and $G(R_7)$ interactions.[41] The phenomenological crystal-field parameters were obtained by a least-squares fit of the calculated energy levels to the experimental energy levels. The theoretical energy levels were obtained using the crystal-field Hamiltonian H_{CEF}

$$H_{CEF}=\sum_{ikq} B_{kq}^{*} C_{kq}(\hat{\mathbf{r}}_i)\ , \tag{8}$$

with $k=2$, 4, 6 and $-k\le q\le k$. B_{kq} are the crystal-field parameters, and the $C_{kq}(\hat{\mathbf{r}})$ are spherical tensors. The sum on i in Eq. (8) covers the three electrons in the $4f^3$ electronic configuration of Nd^{3+}. Since we assume that the Nd^{3+} ions occupy the dodecahedral site with D_2 symmetry, the crystal-field parameters can be chosen real; thus there is a total of nine even-k B_{kq}. In this fitting 9 out of 60 experimental levels were discarded because attempts to fit these levels were unsuccessful.

The positions of the energy levels of Nd:YSAG are quite similar to those of Nd:YAG; consequently, the crystal-field parameters of the latter[17] were chosen as starting parameters in the least-squares fitting. The re-

TABLE V. Experimental (Expt.) and calculated (Theor.) Judd-Ofelt parameters and predicted branching ratios for Nd^{3+}:YSAG and Nd^{3+}:YAG (Refs. 16 and 34). Experimental branching ratios for Nd:YAG from Ref. 39 are given in square brackets.

	Nd^{3+}:YSAG		Nd^{3+}:YAG		
Judd-Ofelt parameters	Expt.	Theor.	Expt. (Ref. 16)	Expt. (Ref. 34)	Theor.
Ω_2 (10^{-20} cm^2)	0.23	0.16	0.37	0.2	0.35
Ω_4 (10^{-20} cm^2)	2.87	1.79	2.29	2.7	2.36
Ω_6 (10^{-20} cm^2)	4.78	10.81	5.97	5.0	13.02
Radiative lifetime					
$^4F_{3/2}$ (μs)	250	173	259	261	128
Branching ratios (%)					
$\beta(^4F_{3/2}\rightarrow{}^4I_{9/2})$	37.8	23	32	37 [25]	21
$\beta(^4F_{3/2}\rightarrow{}^4I_{11/2})$	49.4	62	53	50 [60]	62
$\beta(^4F_{3/2}\rightarrow{}^4I_{13/2})$	12.4	15	15	13 [15]	16
$\beta(^4F_{3/2}\rightarrow{}^4I_{15/2})$	0.4				1

TABLE VI. Experimental crystal-field components A^e_{kq} ($cm^{-1}/Å^k$) and smoothed crystal-field parameters B_{kq} (cm^{-1}) obtained from the B_{kq} of Nd:YSAG.

Ion	B_{20}	B_{22}	B_{40}	B_{42}	B_{44}	B_{60}	B_{62}	B_{64}	B_{66}
A^e_{kq}	3447	239	−332	−3250	−2067	−1019	−506	501	−385
Ce	635	44	−251	−2449	−1558	−2386	−1186	1174	−902
Pr	605	42	−215	−2101	−1336	−1911	−950	940	−722
Nd	588	41	−192	−1877	−1194	−1620	−805	797	−612
Pm	579	40	−177	−1735	−1104	−1449	−720	713	−547
Sm	575	40	−168	−1641	−1044	−1346	−669	662	−509
Eu	574	40	−161	−1572	−1000	−1274	−633	627	−481
Gd	575	40	−155	−1513	−962	−1210	−601	595	−457
Tb	577	40	−149	−1459	−928	−1145	−569	563	−432
Dy	579	40	−144	−1411	−897	−1082	−537	532	−409
Ho	583	40	−140	−1370	−872	−1031	−512	507	−390
Er	588	41	−137	−1341	−853	−1001	−498	493	−378
Tm	594	41	−135	−1317	−838	−983	−489	484	−371
Yb	599	42	−131	−1280	−814	−929	−462	457	−351

sulting parameters that gave the best fit in units of cm^{-1} are

$$B_{20}=588,\ B_{22}=40.8,\ B_{40}=-192\ ,$$

$$B_{42}=-1877,\ B_{44}=-1194,\ B_{60}=-1620\ ,$$

$$B_{62}=-805,\ B_{64}=797,\ B_{66}=-612\ ,$$

with an rms deviation of 9.1 cm^{-1}.

As pointed out by Leavitt,[42] the concept of rotational invariance is a convenient measure of the overall strength of the crystal field for comparison of the resulting B_{kq} for the same ion in different crystals. Here we define the rotational invariants, S_k, by

$$S_k=\left[\sum_{q=-k}^{k} B^*_{kq}B_{kq}\right]^{1/2} \tag{9}$$

for $k=2$, 4, and 6. The values of S_k for Nd:YAG (Ref. 17) and those computed for Nd:YSAG are

$$S_2(\mathrm{YAG})=545\ cm^{-1},\ S_2(\mathrm{YSAG})=591\ cm^{-1}\ ,$$

$$S_4(\mathrm{YAG})=3159\ cm^{-1},\ S_4(\mathrm{YSAG})=3152\ cm^{-1}\ ,$$

$$S_6(\mathrm{YAG})=2548\ cm^{-1},\ S_6(\mathrm{YSAG})=2437\ cm^{-1}\ .$$

Initially, these results are rather surprising in view of the difference in cell size of YAG (a=12.000 Å) and YSAG (a=12.271 Å), which would predict that the YAG crystal-field parameters would be much larger than those of YSAG. However, the distances from the yttrium site to the nearest oxygens are, for YAG 2.303 Å (×4) and 2.432 Å (×4), and for YSAG, 2.338 Å (×4) and 2.440 Å (×4). Since these values are very similar, it is not surprising that the rotational invariants are comparable if it is assumed that the crystal-field parameters are predominately determined by the nearest-neighbor oxygen ions.

In order to calculate the intensity of the electric dipole transitions, we need the odd-k crystal-field components, A_{kq} ($cm^{-1}/Å^k$). In the point-charge model, the crystal-field components are given by[43]

$$A_{kq}=-e^2\sum_j q_j C_{kq}(\hat{\mathbf{R}}_j)/R_j^{k+1}\ , \tag{10}$$

where R_j is the location of the ion with charge q_j (in units of the electronic charge) relative to the rare-earth site. We assume that the charges on the individual ions are $q_Y=3$, $q_{Sc}=3$, and $q_{Al}=-5-4q_0$, with q_0 being the charge on the oxygen ions (note that when q_0 is taken at the valence value −2, q_{Al} is at its valence value of 3). The choice of covalency effects between the oxygen and Al site was made based on the fact that the Al-O distance is very small, 1.77 Å, compared to any other interionic distances (the next smallest distance, Sc-O, is 2.07 Å). In the point-charge model, the crystal-field parameters are given by

$$B_{kq}=\rho_k A_{kq}\ , \tag{11}$$

where the ρ_k are radial factors given by Morrison and Leavitt.[44] Using the values of ρ_k for Nd^{3+}, a set of experimental A^e_{kq} was obtained from the B_{kq} values; these values are given in the top row of Table VI. These experimental A^e_{kq} were used to obtain the best value of q_0 that fit the A_{kq} obtained from Eq. (10). Based on a value of $q_0=-1.79$, the odd-k A_{kq} ($cm^{-1}/Å^k$) from Eq. (10) are $A_{32}=1102$, $A_{52}=-2179$, $A_{54}=1211$, $A_{72}=71.40$, $A_{74}=152.9$, and $A_{76}=-200.3$ (all these odd-k A_{kq} are imaginary).

Having obtained a set of crystal-field components A^e_{kq} by the above procedure, one can obtain a set of crystal-field components for the entire rare-earth series by using Eq. (11). These results are given in Table VI. These B_{kq} can serve as starting parameters for fitting the spectra of any rare-earth ion in YSAG. We referred to the crystal-field parameters obtained by this process as smoothed B_{kq}, since the process is usually used when the experimental data are analyzed on two or more rare-earth ions; in which case the experimental B_{kq} are forced, to a certain degree of consistency, for the entire rare-earth series.

The best-fit B_{kq} and the resulting values of the odd-k A_{kq} were used to calculate the intensity of the electric-

TABLE VII. Calculated Judd-Ofelt intensity parameters Ω_k of rare-earth ions in the Y site of $Y_3Sc_2Al_3O_{12}$.

Ion	JO intensity parameters (10^{-20} cm^2) Ω_2	Ω_4	Ω_6
Ce	0.3031	5.634	46.20
Pr	0.1696	2.846	19.70
Nd	0.1635	1.789	10.81
Pm	0.09461	1.392	8.309
Sm	0.08253	1.172	6.878
Eu	0.06529	0.9122	4.864
Gd	0.05109	0.7031	3.359
Tb	0.08921	1.131	8.146
Dy	0.06270	0.8209	5.055
Ho	0.05357	0.6590	3.691
Er	0.05137	0.6182	3.481
Tm	0.04996	0.5897	3.363
Yb	0.04291	0.4862	2.562

and magnetic-dipole transitions for the rare-earth series. A detailed discussion of this calculation is given by Leavitt and Morrison.[45] The resulting theoretical JO intensity parameters are given in Table VII for the rare earths. In addition, the theoretical JO parameters, manifold-to-manifold branching ratios and radiative lifetime of the $^4F_{3/2}$ state for Nd:YSAG and Nd:YAG are given in Table V.

TABLE VIII. Line-to-line branching ratios (%) of the two levels of the $^4F_{3/2}$ (lines 27 and 28 from Table III) to all the levels of the ^4I_J manifolds ($j=1-26$).

Manifolds	j	E (cm^{-1})	$\beta_{27\to j}$	$\beta_{28\to j}$
$^4I_{9/2}$	1	0	5.8	1.2
	2	114	2.7	3.4
	3	183	1.9	5.3
	4	301	11.5	7.9
	5	823	0.3	0.3
$^4I_{11/2}$	6	1979	22.5	4.6
	7	2022	23.1	12.9
	8	2101	2.9	25.6
	9	2136	3.4	9.8
	10	2437	2.6	5.5
	11	2495	5.5	6.2
$^4I_{13/2}$	12	3905	3.8	4.8
	13	3929	4.0	2.4
	14	4029	2.2	3.7
	15	4044	2.5	2.9
	16	4411[a]	0.4	1.7
	17	4419	1.4	0.4
	18	4478	2.3	0.5
$^4I_{15/2}$	19	5766	0.1	0.4
	20	5797	0.0	0.3
	21	5927	0.3	0.1
	22	5981	0.4	0.1
	23	6544	0.0	0.0
	24	6560	0.1	0.0
	25	6622	0.1	0.1
	26	6711	0.2	0.0

[a]Theoretical level.

The individual Stark-level line strengths for all the crystal-field split levels of the multiplets $^4I_{9/2}$ through $^2G_{9/2}$ were calculated. From these line strengths, the branching ratios for the two levels of the $^4F_{3/2}$ [$E=11\,423$ cm^{-1} (No. 27) and $E=11,523$ cm^{-1} (No. 28)] to the lower ^4I_J ($\frac{9}{2}\le J\le\frac{15}{2}$) crystal-field split levels were determined. The line strengths of the magnetic dipole operators were found to be less than the corresponding electric dipole line strengths by 2 orders of magnitude in almost all the transitions and were ignored in the calculation. In Table VIII we give the branching ratios from both levels of the $^4F_{3/2}$ state to all the levels below. The Sellmeier dispersion equation [Eq. (1)] was used to obtain these results.

G. Laser experiments

A long-pulse laser performance study of Nd:YSAG at 1.06 μm was undertaken using diode array excitation in the side-pump configuration. A diode array capable of producing 475 W in a 300 μs pulse was used as the excitation source. The spectral bandwidth of this array during the entire 300-μs pulse was 2.7 nm FWHM. Additional details of the diode array and experimental procedures have been published previously.[1]

One rod and one straight-through slab were fabricated from the same 6.35-mm-diameter "cored out" stock material by Lightning Optical Corp. (Tarpon Springs, FL). Both materials were 15 mm in length and had appropriate HR and AR coatings centered at 1.06 μm applied on opposite ends. The rod was 6.35 mm in diameter with the barrel polished. The slab was 3 mm thick. AR and HR coatings centered at 808 nm were applied on the side surfaces of the slab and the rod barrel to maximize diode absorption. Using the diode array the absorption coefficient of a Nd:YSAG slab was 5.9 cm^{-1}. This corresponds to 97% absorption of pump radiation in a 6 mm path.

Of the two samples, the slab yielded the better results. The presence of significant optical (index-of-refraction) distortions in both samples was quite evident when the laser cavity was being aligned with a HeNe laser. The rod had an extremely high threshold, and laser oscillation could only be detected with a 99.9% output coupler at an input power of 360 W. The improved performance (lower threshold) of the slab may be attributed to the better geometrical coupling of the two-dimensional diode array to the slab than to the rod. The optical slope efficiencies and extrapolated thresholds for various high-reflectivity output couplers (R) are shown in Table IX for the slab. The round-trip (Findlay-Clay) resonator loss (L) was calculated from the threshold data and was 20%. Since the slope efficiency of a laser (η_s) is proportional to the storage efficiency (η_{storage}) and output coupling efficiency,

$$\eta_s=\eta_{\text{storage}}\frac{1}{1+L/(1-R)}\ , \tag{12}$$

the low slope efficiencies of Nd:YSAG are attributable in large part to the high loss of this material.

TABLE IX. Diode array side-pump laser slope efficiencies and thresholds for Nd:YSAG.

	Output-coupler reflectivity (radius of curvature in parentheses)						
	0.975 (∞)	0.965 (∞)	0.961 (∞)	0.908 (∞)	0.975 (63.5 cm)	0.950 (63.5 cm)	0.915 (75.0 cm)
Optical slope efficiency (%)	4.2	4.6	5.1	5.6	7.6	9.2	8.4
Extrapolated threshold (mJ)	48.1	50.0	52.0	63.2	47.0	53.9	55.1

III. SUMMARY AND CONCLUSIONS

The Judd-Ofelt intensity parameters for Nd:YSAG have been established by two different approaches. The first approach treats the parameters as phenomenological and adjusts them by directly fitting them to the experimentally measured line strengths. The second approach uses the results of a point-charge electrostatic model to predict values for the odd-k A_{kq} terms in the crystal-field expansion and then calculates a set of predicted intensities. Through a least-squares fitting subroutine, the predicted and observed intensities are reconciled and a set of JO parameters is then calculated.

Overall good agreement between observed and calculated intensities eludes both approaches for several reasons. The model does not include dynamic lattice contributions or strain-broadening effects. The measured lifetimes usually include nonradiative contributions in emission. In absorption, multiple (minority) site absorption and phonon sidebands contribute to the measured absorption cross section. For example, in the experimental (first) method, S_{calc} from the ground state to the $^4F_{3/2}$ manifold is larger than S_{meas} for both YAG and YSAG. This leads to a 20% error in the calculated branching ratio to the ^4I_J manifolds in Nd:YAG.[34] On the other hand, this method does predict the radiative lifetime of the $^4F_{3/2}$ state very well, provided the Nd concentration can be accurately determined. The theoretical (second) method predicts too small a radiative lifetime for the metastable state but does predict very well the manifold-to-manifold and line-to-line Stark transitions (see Table V and compare Table VIII to Fig. 2). Additional comparisons of these two models have been published for Nd^{3+} in Y_2O_3.[46]

Slope efficiencies of 47% have been obtained for Nd:YAG using a diode array in the side-pump configuration with thresholds of approximately 20 mJ and losses of approximately 3%.[1] Under similar conditions, our present Nd:YSAG crystal obtained a best slope efficiency of only 9.2%. This is due to the much poorer optical quality of the crystal than is found for Nd:YAG. At high Nd^{3+} concentrations, Nd:YSAG has the advantage over Nd:YAG because the fluorescence lifetime is longer. The lower nonradiative transition rate of Nd:YSAG versus Nd:YAG can be attributed to greater distance between Nd ion pairs in YSAG. This yields fewer ion-ion interactions which quench the fluorescence. Thus, if more effort can be given to improving the optical quality of YSAG, as has been done for YAG, the Nd:YSAG crystal is potentially a better Q-switch laser than Nd:YAG.

ACKNOWLEDGMENTS

The Science Applications International Corporation (SAIC) gratefully acknowledges financial support from the Center for Night Vision and Electro-Optics. The authors thank Dr. C. F. Campana for the crystal structure solution, R. Phillips and W. Hovis for the elemental analysis on YSAG, V. King for technical assistance in the lifetime determination, L. Thompson for polishing samples, and Dr. L. Merkle for reviewing the manuscript. J.B.G. wishes to thank the American Society for Engineering Education for their support, and Dr. M. E. Hills, Chemistry Division, Naval Weapons Center, China Lake, California, for many helpful discussions and encouragement.

[1] T. H. Allik, W. W. Hovis, D. P. Caffey, and V. King, Opt. Lett. **14**, 116 (1989).
[2] J. Berger, D. F. Welch, D. F. Scifres, W. Streifer, and P. Cross, Electron. Lett. **23**, 669 (1987).
[3] B. Zhou, T. J. Kane, G. J. Dixon, and R. L. Byer, Opt. Lett. **10**, 62 (1985).
[4] R. A. Fields, M. Birnbaum, and C. L. Fincher, Appl. Phys. Lett. **51**, 1885 (1987).
[5] F. Hanson and D. Haddock, Appl. Opt. **27**, 80 (1988).
[6] F. Hanson and G. Imthurn, IEEE J. Quantum Electron. **QE-24**, 1811 (1988).
[7] J. B. Gruber, M. E. Mills, C. A. Morrison, G. A. Turner, and M. R. Kokta, Phys. Rev. B **37**, 8564 (1988).
[8] R. Burnham and A. D. Hayes, Opt. Lett. **14**, 27 (1989).
[9] A. L. Denisov, E. V. Zharikn, A. I. Zagumennyi, S. P. Kalitin, V. A. Smirnov, A. I. Talybov, and I. A. Shcherbakov, Zh. Prikl. Spektrosk. **49**, 430 (1988).
[10] A. A. Kaminskii, *Laser Crystals* (Springer, New York, 1981).
[11] A. G. Avanesov, A. A. Danilov, A. L. Denisov, E. V. Zharikov, A. I. Zagumennyi, O. V. Kuz'min, M. Yu. Nikol'skii, V. G. Ostroumov, V. F. Pisarenko, Academician A. M. Prokhorov, V. A. Smirnov, I. T. Sorokina, E. V. Tumaev, and I. A. Shcherbakov, Dokl. Akad. Nauk. SSSR **292–297**, 1098 (1987) [Sov. Phys.—Dokl. **32**, 665 (1987)].

[12]Kh. S. Bagdasarov, A. A. Kaminskii, A. M. Kevorkov, and A. M. Prokorov, Dokl. Akad. Nauk. SSSR **214–219**, 810 (1974) [Sov. Phys. Dokl. **19**, 671 (1975)].
[13]M. Kokta, J. Solid State Chem. **8**, 39 (1973).
[14]C. D. Brandle and R. L. Barns, J. Crystal Growth **20**, 1 (1973).
[15]V. F. Kitaeva, E. V. Zharikov, and I. L. Chistyi, Phys. Status Solidi A **92**, 475 (1985).
[16]A. A. Kaminskii and L. Li, Phys. Status Solidi A **26**, K21 (1974).
[17]C. A. Morrison and R. P. Leavitt, in *Handbook of the Physics and Chemistry of Rare Earths,* edited by K. A. Gschneidner, Jr. and L. Eyring (North-Holland, New York, 1982), Vol. 5, pp. 461–684.
[18]G. Huber, E. W. Duczynski, P. Mitzscherlich, and H. O. Teichmann, J. Phys. **48**, C7-309 (1987).
[19]E. W. Duczynski, H. J. v.d. Heide, G. Huber, P. Mitzscherlich, K. Petermann, and H. O. Teichmann in *Cr,Nd:YSAG: A New Sensitized Garnet Laser with Increased Repetition Rate Capability,* Proceedings of the International Conference on Lasers and Electro-Optics, 1989 Technical Digest Series, Vol. 11 (Optical Society of America, Washington, D.C. 1989) pp. 110-111.
[20]B. R. Judd, Phys. Rev. **127**, 750 (1962).
[21]G. S. Ofelt, J. Chem. Phys. **37**, 511 (1962).
[22]C. A. Morrison, N. Karayianis, and D. E. Wortman, Harry Diamond Laboratories Technical Report No. HDL-TR-1816, 1977 (unpublished).
[23]L. G. Morozova and P. P. Feofilov, Izv. Akad. Nauk. SSSR, Neorg. Mater. **4**, 1738 (1968).
[24]C. D. Brandle and J. C. Vanderleeden, IEEE J. Quant. Elec. **QE-10**, 67 (1974).
[25]D. Pruss, G. Huber, A. Belmowski, V. V. Laptev, I. A. Scherbakov, and Y. V. Zharikov, Appl. Phys. B **28**, 355 (1982).
[26]R. Phillips, Kevex Instruments, 50 Valley Stream Parkway, Malvern, PA 19355 (unpublished).
[27]G. A. Bogomolova, L. A. Bumagina, A. A. Kaminskii, and B. Z. Malkin, Fiz. Tverd. Tela (Leningrad) **19**, 2439 (1977) [Sov. Phys.—Solid State **19**, 1428 (1977)].
[28]C. F. Campana, Nicolet X-ray Division, 5225-5 Verona Road, Madison, WI 53711 (unpublished).
[29]W. L. Bond, J. Appl. Phys. **36**, 1674 (1965).
[30]S. H. Wemple and W. J. Tabor, J. Appl. Phys. **44**, 1395 (1973).
[31]J. B. Gruber, M. E. Hills, T. H. Allik, C. K. Jayasankar, J. R. Quagliano, and F. S. Richardson (unpublished).
[32]J. D. Axe, J. Chem. Phys. **39**, 1154 (1963).
[33]W. F. Krupke and J. B. Gruber, Phys. Rev. **139**, A2008 (1965).
[34]W. F. Krupke, IEEE J. Quantum Electron.**QE-7**, 153 (1971).
[35]W. F. Krupke, M. D. Shinn, J. E. Marion, J. A. Caird, and S. E. Stokowski, J. Opt. Soc. Am. B **3**, 102 (1986).
[36]M. J. Weber, T. E. Varitmos, and B. M. Matsinger, Phys. Rev. B **8**, 47 (1973).
[37]T. S. Lomheim and L. G. DeShazer, J. Appl. Phys. **49**, 5517 (1978).
[38]T. S. Lomheim and L. G. DeShazer, Phys. Rev. B **20**, 4343 (1979).
[39]E. Comperchio, M. Weber, and R. Monchamp, *High Quality Nd:YAG Laser Materials,* U.S. Army Electronics Command, Fort Monmouth, NJ Report No. DAAB07-69-C-0227, 1970 (unpublished).
[40]T. H. Allik, S. A. Stewart, D. K. Sardar, G. J. Quarles, R. C. Powell, C. A. Morrison, G. A. Turner, M. R. Kokta, W. W. Hovis, and A. A. Pinto, Phys. Rev. B **37**, 9129 (1988).
[41]B. G. Wybourne, *Spectroscopic Properties of Rare Earths* (Wiley, New York, 1965). The free-ion parameters E^k, α, β, γ, and ζ are given in Ref. 40.
[42]R. P. Leavitt, J. Chem. Phys. **77**, 1661 (1982). The relationship of the S_k used in the text and the S of Leavitt's is $S=[(\frac{1}{3}\sum_k S_k^2/2k+1)]^{1/2}$.
[43]C. A. Morrison, *Angular Momentum Theory Applied To Interactions in Solids,* Vol. 47 of *Lecture Notes in Chemistry* (Springer-Verlag, New York, 1988).
[44]C. A. Morrison and R. P. Leavitt, J. Chem. Phys. **71**, 2366 (1979).
[45]R. P. Leavitt and C. A. Morrison, J. Chem. Phys. **73**, 749 (1980).
[46]C. A. Morrison, R. P. Leavitt, J. B. Gruber, and N. C. Chang, J. Chem. Phys. **79**, 4758 (1983).